Photodegradation of thiophanate-methyl under simulated sunlight by utilization of novel composite photocatalysts

Aleksandar A. Jovanović[1], Mladen D. Bugarčić[1], Miroslav D. Sokić[1], Tanja S. Barudžija[2], Vladimir P. Pavićević[3] and Aleksandar D. Marinković[3]

[1]*Institute for Technology of Nuclear and Other Mineral Raw Materials, Belgrade, Serbia*
[2]*University of Belgrade, "VINČA" Institute of Nuclear Sciences - National Institute of the Republic of Serbia, Belgrade, Serbia*
[3]*University of Belgrade, Faculty of Technology and Metallurgy, Belgrade, Serbia*

Abstract

This work aimed to investigate the influence of modified titanium(IV) oxide by different nanosized particles on photocatalytic capacity to decompose the chosen organic pollutant under simulated sunlight. For that purpose, rutile-phased titanium(IV) oxide (r-TiO_2) was decorated with iron vanadate ($FeVO_4$/r-TiO_2) and vanadium-substituted goethite ($Fe_{1-x}V_xOOH$/r-TiO_2). The obtained composites were characterized by field emission scanning electron microscopy, energy-dispersive X-ray spectroscopy, X ray powder diffraction, Brunauer-Emmett-Teller, Fourier transform infrared spectroscopy – attenuated total reflectance and ultraviolet–visible diffuse reflectance spectroscopy techniques. Both synthesized photocatalysts showed higher photoactivity than the base r-TiO_2 for the degradation of the target contaminant - thiophanate-methyl (2.5 h *vs*. 5 h). During the tests, parameters like the irradiation time, catalysts amount, and pesticide concentration were systematically investigated. Furthermore, photocatalysts were applied in multicycle degradation tests for examining their effectiveness during exploitation time. Monitoring of the removal rate was performed both by UV/visible spectrometry and high-performance liquid chromatography (HPLC). In order to prove completion of fungicide degradation chemical oxygen demand was measured in the course of the photocatalytic experiment. The final concentration of the observed contaminant in treated samples was under the prescribed legislative level. The fabricated materials displayed great reliability, durability and photocatalytic activity representing good potentials for implementing this process in real wastewater treatment plants.

Keywords: photocatalysis; titanium(IV) oxide; advanced oxidation process; pesticide pollution; wastewater.

Available on-line at the Journal web address: http://www.ache.org.rs/HI/

ORIGINAL SCIENTIFIC PAPER

UDC: 577.152.3:544.478.3

Hem. Ind. **00(0)** 000-000 (2024)

1. INTRODUCTION

Contamination of the environment with different classes of organic pollutants is constantly increasing [1,2]. Several types of pesticides were employed as agents in agriculture production and preservation[3-5]. One of them is thiophanate-methyl, a fungicide with immense usage predominantly in the area of inhibition of fungal growth and extension of the product life. The induced negative side effects on public health and non-target organisms presented in previous investigations[6-8] made this fungicide forbidden by the legislative [9]. However, it can be still found on the market, and it has been also detected in water sources [10].

Treatment of pesticide-contaminated waters originating from industrial plants or agricultural fields can be performed in many ways [11,12]. The most promising techniques nowadays are advanced oxidative processes (AOPs), where photocatalysis has almost a mandatory role. Different organic and inorganic-based materials are utilized as photocatalysts with the aim to promote the decomposition of various pollutants [13,14]. Rapid production of complex, persistent organic hazardous chemicals has caused an increased demand for enhanced photosensitive materials that can catalyze pollutant decomposition over their surfaces. A predominantly used photocatalyst is TiO_2, with its structural

Corresponding authors: : Aleksandar A. Jovanović, Institute for Technology of Nuclear and Other Mineral Raw Materials, Belgrade, Serbia
E-mail: a.jovanovic@itnms.ac.rs
Paper received: 25 May 2023; Paper accepted: 6 January 2024; Paper published: 25 January 2024.
https://doi.org/10.2298/HEMIND230523004J

modifications [15]. These catalysts provide outstanding potentials for boosting the degradation of organic pollutants in wastewater due to their good physicochemical properties [16].

Heterojuncted materials exhibit exceptional performances as a faster electron/hole separation, great stability, decreased degradation time and lower band gap energy [17,18]. Transition metal oxides contain smaller band gaps, such as vanadium compounds, which can be combined with TiO_2 to create a heterojunction complex. Progress in charge carrier separation can be achieved by minimizing recombination throughout photocatalysis [19]. Recently, iron vanadate was used in the sphere of electrocatalysis, photoluminescence, optical and humidity sensors, *etc*. [20]. It was found that $FeVO_4$ doping with different transition metal cations and commercial TiO_2 P25 truly improve material properties [21,22]. Hence, it is anticipated that adding $FeVO_4$ to rutile TiO_2 will enhance the stability and selectivity of such a novel catalyst. On the other hand, vanadium-substituted goethite ($Fe_{1-x}V_xOOH$) appears as a promising adsorbent in wastewater treatment, but it was not tested as a catalyst. A major disadvantage of application photocatalysis is the price of prepared photocatalysts, mostly due to the usage of costly nanosized photocatalysts.

The purpose of this study was to investigate removal and degradation efficiency of the fungicide thiophanate-methyl from water solutions by photocatalysis under simulated sunlight. Two newly fabricated photocatalysts based on commercial r-TiO_2, *i.e*. $FeVO_4$/r-TiO_2 and $Fe_{1-x}V_xOOH$/r-TiO_2 were structurally analyzed and utilized comparatively as photocatalysts. This study aims to propose the preparation of photoactive and low-cost rutile-based catalysts that possess decent oxidation properties. From the literature review, the abovementioned composites were not yet fabricated and applied in this way.

2. EXPERIMENTAL

2. 1. Materials

In order to develop photocatalysts, various chemicals were utilized. The surface of rutile-phased TiO_2(r-TiO_2, Sigma Aldrich, Germany) was modified by the deposition of oxides and hydroxides in the system water layer around r-TiO_2 and non-solvent medium (xylene, 98 %, Zorka Pharma, Serbia) to perform effective deposition of iron vanadate ($FeVO_4$/r-TiO_2) and vanadium-substituted goethite ($Fe_{1-x}V_xOOH$/r-TiO_2). Pesticide thiophanate-methyl - TPM (purity > 95 %) was acquired from Agrosava, Serbia. Hence, the used chemicals for surface modification were: $Fe(NO_3)_3\times 9H_2O$ (*p. a.* Fisher, UK), NH_4VO_3(*p. a.* Merck, Germany), VCl_3 (*p. a.* Sigma Aldrich, Germany), ethanol (96 %, Reahem, Serbia), KOH (*p. a.* Zorka, Serbia). All solutions were prepared with deionized water (18.2 MΩ cm).

The surfaces of both catalysts were enriched to approximately 5 wt.% of $FeVO_4$ and $Fe_{1-x}V_xOOH$ regarding the initial r-TiO_2 mass.

2. 2. Synthesis of $FeVO_4$/r-TiO_2

In a 50 cm^3 three-necked pyrex flask, equipped with a refluxed condenser, thermometer and air inlet tube, 2.00 g r-TiO_2 and 0.0753 g NH_4VO_3 were added and mixed in 4.00 mL of deionized water. The prepared pasty suspension was overlaid with 12.00 mL of xylene and heated at 70 °C for 1 h. Subsequently, 2 mL of $Fe(NO_3)_3\times 9H_2O$ (m = 0.2602 g) solution was added dropwise to the solution and heated at 70 °C for 1 h without mixing. Thereafter, the obtained composite was rinsed with deionized water and ethanol (2 times), centrifuged, and dried for 6 h. In the last step, the composite was annealed at 520 °C for 4 h.

2. 3. Synthesis of $Fe_{1-x}V_xOOH$/r-TiO_2

r-TiO_2 powder (2.00 g) and 10.00 mL of xylene were added in a 50 mL three-necked flask. Then, a water solution of 0.7503 g of VCl_3 and 0.4289 g $Fe(NO_3)_3\times 9H_2O$ were added together with 2.50 mL of deionized water. The solution was mixed for 1 h at 70 °C. After 1 h, 1.5 mL of a 15 M solution of KOH was added and stirred for an additional hour. The prepared solution was stored in the dark for 15 days to obtain particles with smaller diameters (in contrast to 48 days according to Schwertman & Cornell [23]). Lastly, the stored solution was rinsed with ethanol and deionized water until negative chloride reaction and dried for 2 h at 60 °C.

2. 4. Structural characterization of prepared composites

Presence of crystalline phases in commercial and two modified materials was determined based on measurements using SmartLab Rigaku powder diffractometer (Rigaku, Japan) that works on the principle of Bragg-Brentano geometry, using an X-ray tube with a copper anticathode, *i.e.* using CuKα radiation of wavelength λ = 0.154178 nm. The voltage on the X-ray tube was 40 kV, and the current was 30 mA. Measurements were made in the range of diffraction angles 2 θ from 10 to 80° with a step of 0.02° and a measurement speed of 1° min^{-1}. The Brunauer-Emmett-Teller (BET) technique was utilized to estimate the specific surface area of photocatalysts, by Micrometrics ASAP 2020 (Micromeritics Instrument Corporation, USA). The identification of functional groups in base and modified materials was authenticated by Fourier-transform infrared spectroscopy with Attenuated total reflection (ATR-FTIR) using Nicolet iS 10 FTIR Spectrometer (ThermoFisher Scientific, USA). Spectra were collected in the range 4000 to 400 cm^{-1}. Analysis of particle surface morphology was examined by a Field Emission Scanning Electron Microscope (FE-SEM) TESCAN MIRA 3 (TESCAN ORSAY HOLDING, a.s., Czech Republic). Mapping of photocatalyst surfaces was performed by FE-SEM JSM 7001F (Jeol, Japan) coupled with an energy dispersive spectrometer (EDS) Xplore 15 (Oxford Instruments, UK) operated at accelerating voltage of 20 kV, probe current of 10 nA in high vacuum mode (0.1 mPa). Optical properties of base and fabricated composites were determined by UV-Vis diffuse reflectance spectroscopy (UV-DRS) (Shimadzu UV-Vis UV-2600, Japan). Determination of band gap energies will give a better insight into photocatalytic activity.

2. 5. Photocatalytic tests

A water solution of thiophanate-methyl (TPM) was placed in a 200 mL cylindrically shaped quartz reactor together with a photocatalyst at room temperature. The TPM solution (150 mL) and selected photocatalyst (67 mg L^{-1}) was mixed in the dark for 30 min at 200 rpm on a magnetic stirrer (IKA C-MAG HS7, IKA, China) with the aim to achieve adsorption-desorption equilibrium among the prepared solution and chosen photocatalyst and the reactor was temperature controlled by the feedback loop. Immediately afterward, the source of irradiation (Osram Vitalux, Germany, 300 W, UVA:UVB = 13.6:3) was placed 20 cm above the solution level in the reactor and degradation was initiated. Light intensity of the light source was determined previously [24].

Equation (1) was used to evaluate the degradation or pesticide removal (*PR*):

$$PR = \frac{c_i - c_f}{c_i} 100 \quad (1)$$

where c_i and c_f represent the initial and the final pesticide concentration, respectively. Furthermore, endurance and efficiency of the fabricated materials were estimated in five consecutive cycles. Before each application, catalysts were collected from the solution, rinsed and centrifuged with ethanol and deionized water.

The photocatalytical experiments were performed in triplicates, for attenuating measurement uncertainty.

2. 6. Analytical procedures

Monitoring of fungicide degradation was recorded by UV/Vis spectroscopy (Shimadzu 1800, Japan) and high pressure liquid chromatography (HPLC) (Dionex UltiMate 3000 LC system, Thermo Fisher Scientific, USA with Zorbax Eclipse XDB-C18, 250 × 4.6 mm (i.d.) × 5 µm column, mix of methanol (25 %), acetonitrile (25 %) and water (50 %) as eluent). Every 30 min up to 5 h water aliquots (3.00 mL) were sampled, filtered through a 0.25 µm syringe filter and placed into a cuvette. Further, the kinetic rate constant (*k*) from all degradation reactions was determined together with halftime periods ($t_{1/2}$), by using the pseudo-first order kinetic model:

$$\ln \frac{c_t}{c_i} = -kt \quad (2)$$

$$t_{½} = \frac{\ln 2}{k} \quad (3)$$

where c_i and c_t are the initial and the pesticide concentration at some time *t*, respectively. As a check-up, the concentrations were also measured by HPLC.

2. 7. Environmental impact

Evaluation of oxygen consumption of initial molecules and their fractions during the degradation process represents a necessary step in the evaluation of the efficiency and eco-friendliness of the implemented treatment process. Chemical oxygen demand (COD) was determined by the EPA [25] standard method. The obtained values were compared with those given in the legal regulations.

3. RESULTS AND DISCUSSION

3. 1. Structural characterization of prepared composites

SEM micrographs of all investigated photocatalysts are presented in Figure 1.

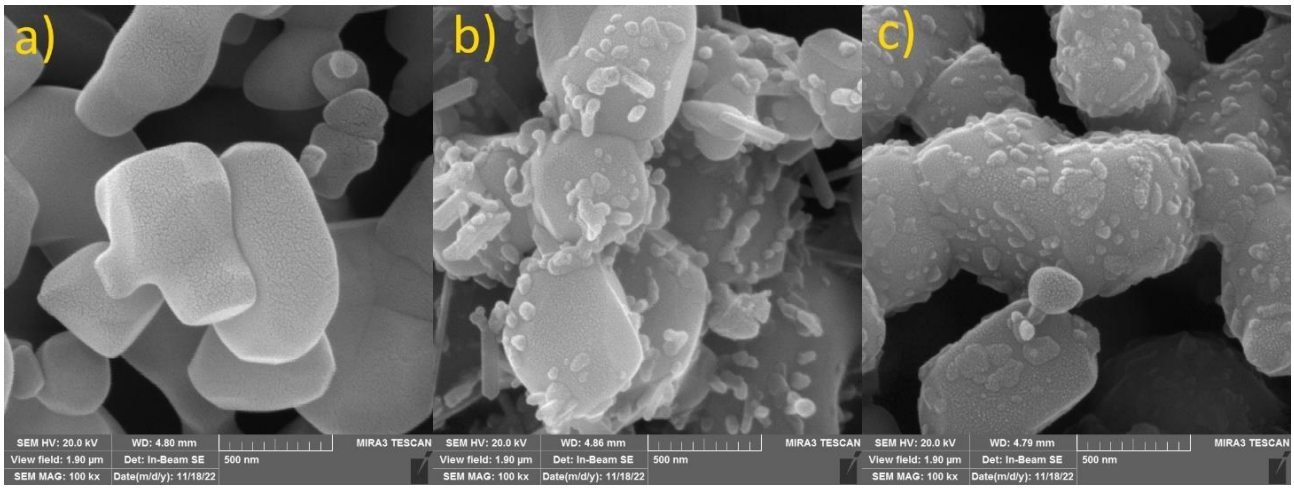

Figure 1. FE SEM micrographs of: a) r-TiO_2, b)$FeVO_4$/r-TiO_2 and c) $Fe_{1-x}V_xOOH$/r-TiO_2 (scale bar = 500 nm)

Particles seen in Figure 1a present the base material which is consistent with the rutile phase TiO_2. The particles have smooth surfaces and uneven shape. The smallest particle diameter is about 0.5 µm, while the largest length is about 5 µm (the data are provided by the manufacturer obtained from sieves analysis).

The material modified with $FeVO_4$ (Fig. 1b) differs from the base one since the surface of rutile TiO_2 is decorated by deposed particles ($FeVO_4$). The iron vanadate particles are mostly rod-shaped (length x diameter = 200 nm × 50 nm) or coerced nanoparticles (mostly cubic with edges ≈ 50 nm) [26,27]. The presence of those particles contributes to a negligible increase in the specific surface area (SSA) from 0.54 $m^2 g^{-1}$ for r-TiO_2, to 1.70 $m^2 g^{-1}$ obtained for $FeVO_4$/r-TiO_2. as determined by the BET method.

The presence of V-substituted goethite on the surface of the sample ($Fe_{1-x}V_xOOH$) can be seen in Figure 1c. Those particles are uniformly deposited and are in the shape of flakes, rarely found as sticks. All deposed particles exhibit pox-like surfaces. A similar shape of fabricated oxyhydroxide particles is observed with other transition metals, as reported in literature [28,29]. Dimension of deposited particles is in the range from 50 nm for single particles to 250 nm for coerced flakes, while the sticks are 50 nm in diameter and up to 200 nm in length. The SSA of $Fe_{1-x}V_xOOH$-modified material is 1.82 $m^2 g^{-1}$.

Surface mapping of fabricated materials is shown in Figures 2 and 3.

SEM-EDS analyses have shown four elements on the surfaces of the prepared photocatalysts. Oxygen, titanium, iron and vanadium constitute both materials in different portions. The ratio of presented elements in Figure 2 are: 32.11 wt.% Ti, 66.64 wt.% O, 0.79 wt.% Fe, 0.47 wt. % V, while in Figure 3 are: 32.41 wt.% Ti , 66.35 wt.% O, 1.06 wt.% Fe, 0.19 wt.% V. The distribution of mentioned elements in Figures 2 and 3 confirms that deposition of nanoparticles on TiO_2 surface is achieved. The calculations verified that the deposited amount of $FeVO_4$ was 5.14 wt.% and $Fe_{1-x}V_xOOH$ was 4.27 wt.%, from scans on Figures 2 and 3.

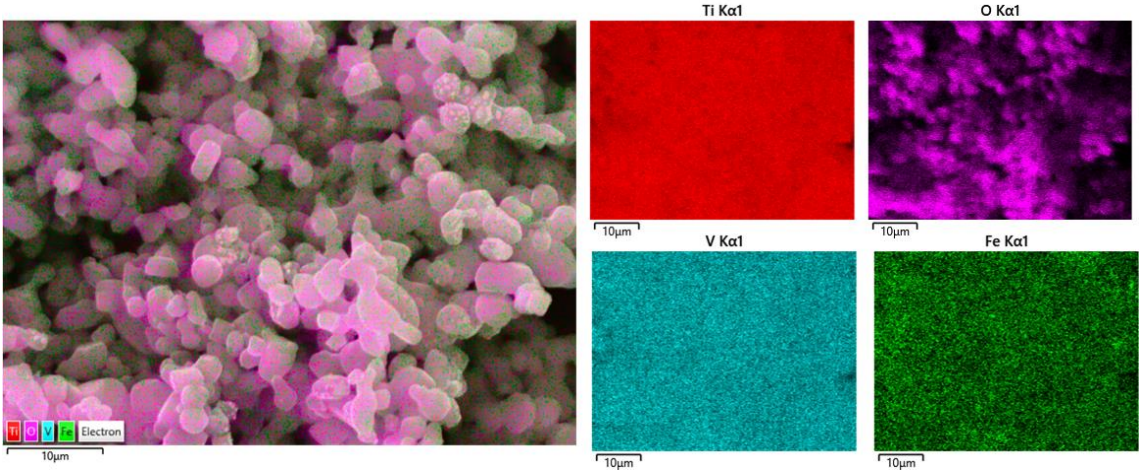

Figure 2. EDS mapping of $FeVO_4$/r-TiO_2 surface (detector for Secondary Electron Imaging, Working Distance 4.80 mm)

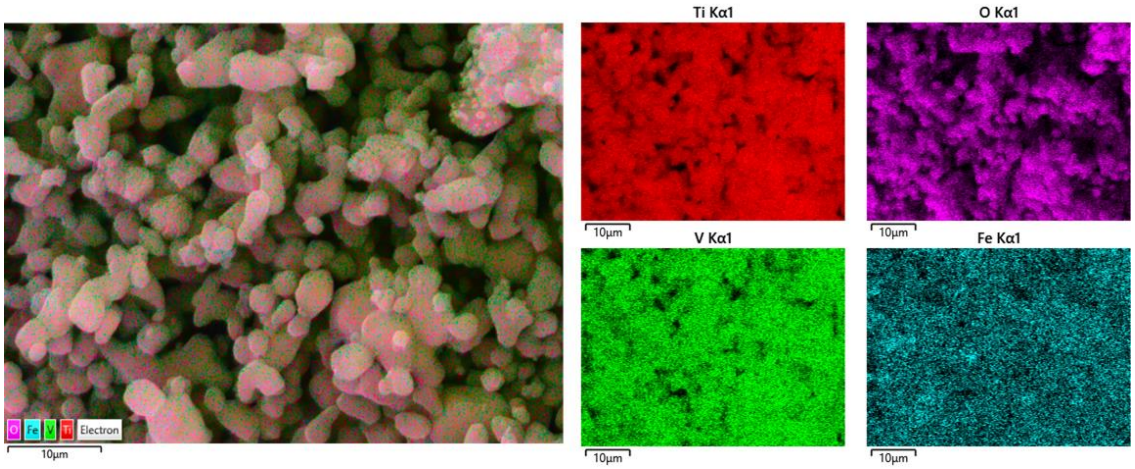

Figure 3. EDS mapping of $Fe_{1-x}V_xOOH$/r-TiO_2 surface (detector for Secondary Electron Imaging, Working Distance 4.80 mm)

The phase compositions of the base and prepared photocatalysts are shown in Figure 4.

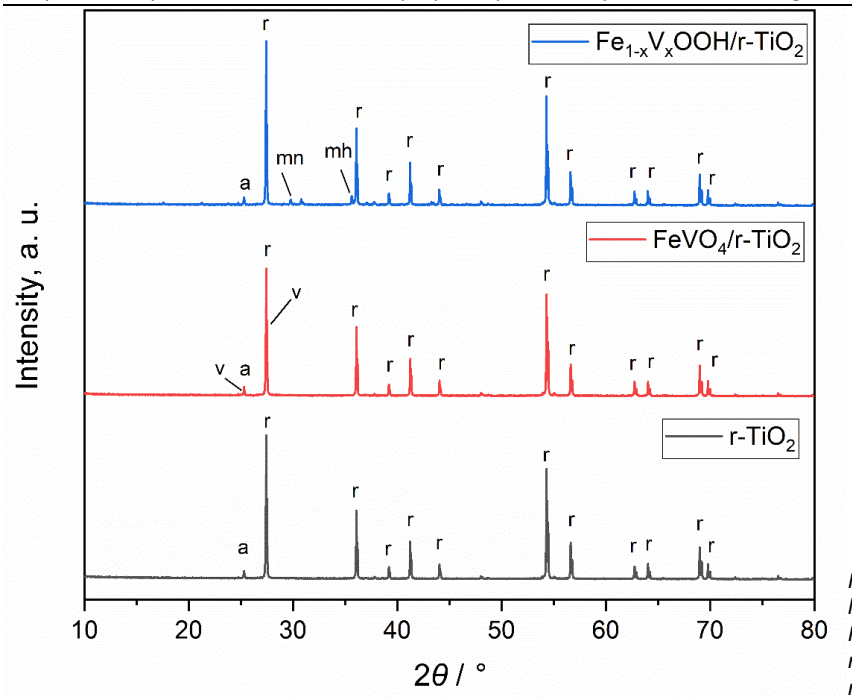

Figure 4. XRPD patterns of r-TiO_2 (bottom line), $FeVO_4$/ r-TiO_2 (middle line) and $Fe_{1-x}V_xOOH$/r-TiO_2 (upper line); r - rutile, a - anatase, mn - magnetite, mh - maghemite, v -iron(III) vanadate

The base material (black line in Fig. 4) is mostly composed of rutile phase TiO_2 particles (observed peaks at 27.4, 36.1, 39.2, 41.2, 44.0, 54.3, 56.6, 62.8, 64.0, 69.0 and 69.8°, PDF No. 03-065-0191) with the small amount of anatase phase (most pronounce peak at 25.3°, PDF No. 01-086-1157). Both fabricated materials have similar peaks as the start material. The XRPD pattern of $Fe_{1-x}V_xOOH/r\text{-}TiO_2$ (upper spectrum in Fig. 4) contains additional diffraction peaks at: 35.6° that could be ascribed to maghemite (PDF No. 01-089-5892), 29.7° that could be ascribed to magnetite (PDF No. 01-089-0951) and 30.8° that could be assigned to brookite (PDF No. 01-076-1934) [30]. The XRPD pattern of $FeVO_4/r\text{-}TiO_2$ (middle spectrum Fig. 4) contains additional small peaks at 25.0 and 27.7° that belong to $FeVO_4$ (PDF No. 00-038-1372) [31] that coincides with the most intensive peak of anatase and rutile phase, respectively [32].

The FT-IR spectra of $r\text{-}TiO_2$, $FeVO_4/ r\text{-}TiO_2$ and $Fe_{1-x}V_xOOH/ r\text{-}TiO_2$ particles are shown in Figure 5.

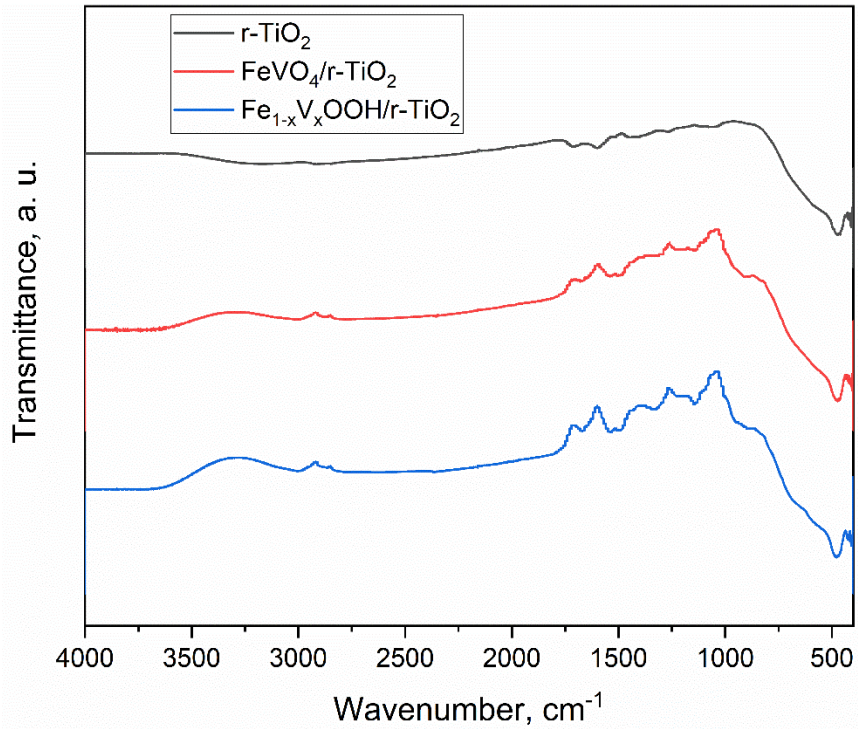

Figure 5. ATR-FTIR spectra of $r\text{-}TiO_2$(upper spectrum), $FeVO_4/ r\text{-}TiO_2$(middle spectrum) and $Fe_{1-x}V_xOOH/r\text{-}TiO_2$ (bottom spectrum)

By observing the FTIR spectra of the two synthesized materials, several new peaks are found. Firstly, a broad peak in a range from 930 to 890 cm^{-1} was attributed to V=O and V-O-V coupled vibrations as well as the stretching of vanadyl (V=O) bonds, respectively [31]. Due to intense Ti-O vibrations in $r\text{-}TiO_2$, combined bridging and stretching of V-O-Fe were overlapped [31]. According to the peak found at 505 cm^{-1}, V-O-V deformation vibration together with Fe-O stretching modes is observed [33].

One of the parameters of utmost significance for improvement of photocatalytic activity is achievement of a lower band gap energy (E_{gap}). The quantity of deposited $FeVO_4$ and $Fe_{1-x}V_xOOH$ (~5 wt.%) and contact between phases caused changes in the material electronic configuration. DRS and Tauc graphics for the two synthesized materials are presented in Figure 6. E_{gap} values were retrieved by Tauc plot, obtained by charting $(F(R)hv)^n$ *vs.* hv, where R is reflectance and $F(R)$ is the so-called remission or Kubelka-Munk function, n = 1/2.

The obtained band gap energies of all investigated materials are listed in ascending order: 2.68, 2.87 and 3.03 eV for $Fe_{1-x}V_xOOH/r\text{-}TiO_2$, $FeVO_4/r\text{-}TiO_2$ and $r\text{-}TiO_2$, respectively. The determined E_{gap} values indicate that the presence of particles on the surfaces of rutile microparticles induces lowering the energy needed for excitation [34]. By decreasing the energy gap in heterojuncted photocatalysts, the surface electron - hole transition is facilitated. This phenomenon induces faster generation of oxidative species and decreases the degradation time.

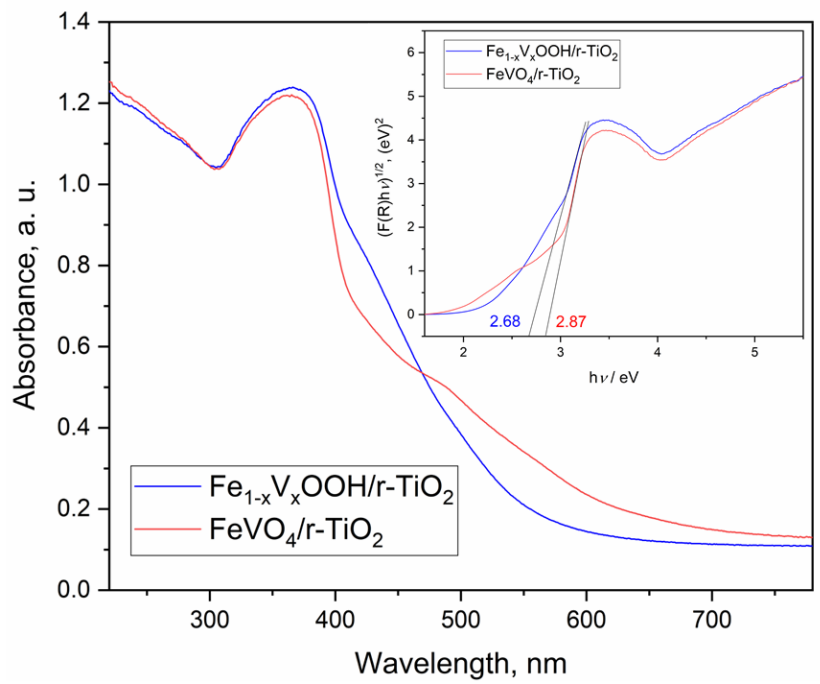

Figure 6. DRS and Tauc plots for $FeVO_4$/ r-TiO_2 and $Fe_{1-x}V_xOOH$/r-TiO_2

3. 2. Photocatalytic assays

Process parameters have to be investigated prior to any possible application of a process on the pilot level. The obtained results in essential tests in this area of engineering are presented in the following lines.

3. 2. 1. Photocatalyst mass

When the mass of the applied catalyst is considered, it should be taken into account that a higher mass does not mean a better result within the observed system. Namely, when the amount of catalyst is very low, the total number of active centers on the surface that could generate electron/hole pair (*i.e.* reactive radicals in solution which participate in degradation of the present pollutant) is not sufficient to perform photodegradation at a satisfactory rate. On the other hand, an excessive amount of catalyst leads to its potential coagulation and precipitation. In addition, a large catalyst amount hinders penetration of radiation into the pollutant and catalyst solution suspension, thereby reducing the efficiency of the process and the inevitable prolongation of the reaction. Effects of catalyst amount on photocatalytic efficiency are shown in Figure 7.

As can be seen in Figure 7, the best results were obtained when the catalyst amount was 10 mg (150 mL)$^{-1}$ (67 mg L^{-1}). This dosage of catalyst (*i.e*. 67 mg L^{-1}) was used in the following tests as the optimal for removal of TPM. In our previous work (Jovanovic et al., 2023), a photolytic test was performed under the same experimental conditions (initial TPM concentration and irradiation time)[35]. The findings indicated that the photolytic degrading efficiency was extremely poor. Namely, the results demonstrated that photocatalytic rates for 5 and 10 mg L^{-1} of TPM was 33 and 23 times higher, respectively, then photolytic decomposition [35]. Furthermore, adsorption tests were conducted in dark, by addition of the chosen photocatalyst in a TPM solution resulting in a slight decrease in the TPM concentration by a maximum of 10 %. The obtained findings implied that adsorption is not the primary process during the complete photocatalysis. Effectiveness of the interaction between TPM and photocatalyst significantly determines the further reaction kinetic. Obviously, the additional obstacle is the cost of the used catalyst, and from that side it is necessary to further optimize the process as much as possible.

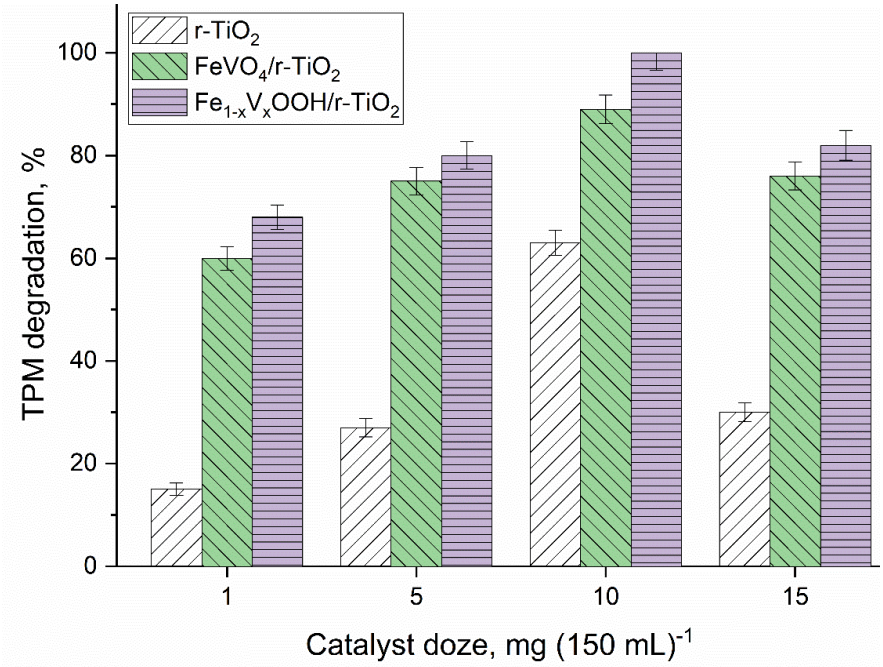

Figure 7. Impact of the catalyst amount on the TPM removal efficiency (c_0 = 5 mg L^{-1}, t = 150 min, 200 rpm; data are the average of n = 3)

3. 2. 2. Initial pollutant concentration

The second factor that directly affects the process rate is the initial TPM concentration. The influence of varied concentrations of TPM on degradation profiles is shown in Figure 8. Low solubility of TPM in water (18.5 mg L^{-1} at 20 °C) defines the upper limit of the fungicide concentration [36]. By observing the TPM degradation curves in the initial concentration range 1 to 15 mg L^{-1}, it can be seen that degradation efficiency gradually decreases. This can be explained by lower free spots on the catalyst surface for the generation of hydroxyl radicals.

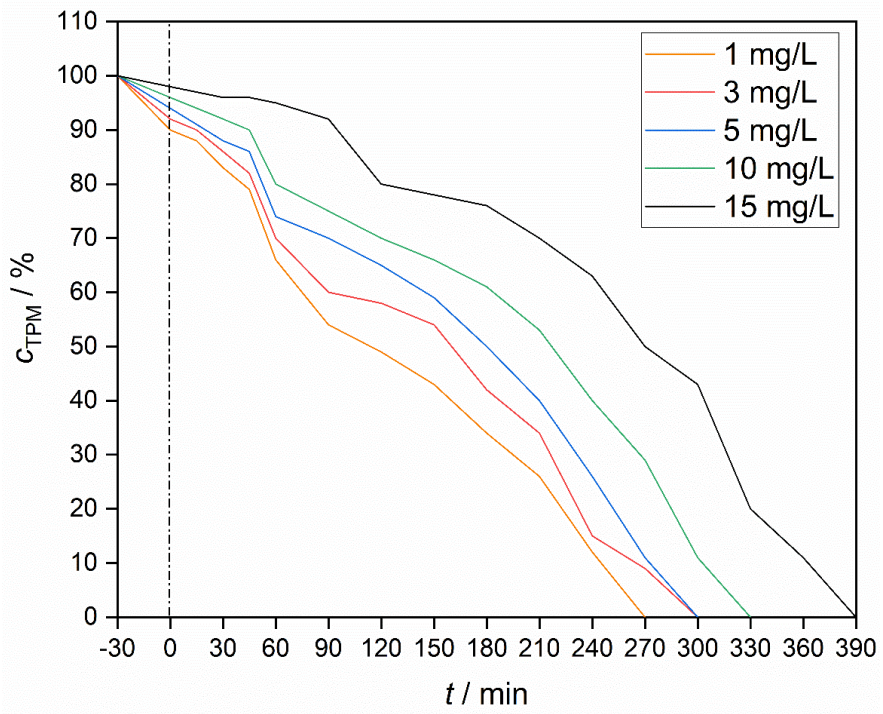

Figure 8. Influence of the initial TPM concentration on the degradation percentage (150 mL of suspension mixing at 200 rpm in the dark for the first 30 min, after that mixing under irradiation using 0.067 g L^{-1} r-TiO_2)

Complete degradation of TPM was accomplished in 5 h for the systems with the initial concentrations of 3 and 5 mg L^{-1} . At the lower initial concentration of 1 mg L^{-1} even a shorter degradation time was obtained. Longer irradiation times were necessary at higher TPM concentrations (10 and 15 mg L^{-1}) to achieve the complete pollutant degradation. It was decided that the optimal initial concentration for the photocatalytic probes was 5 mg L^{-1}, and similar concentration was also detected in riverside, as reported in literature [10].

The calculated values of reaction rate constant (k) and half-time ($t_{1/2}$) for TPM degradation at different initial concentrations are given in Table 1.

Table 1. Estimated kinetic rate constant (k) and degradation half-time ($t_{1/2}$) for TPM

TPM concentration, mg L^{-1}	k±SE* /10^4 min^{-1}	$t_{1/2}$ / min	R^2
1	59.4±3.5	117	0.963
3	45.6±3.5	152	0.939
5	35.9±2.4	193	0.950
10	29.7±1.4	233	0.964
15	18.6±1.0	273	0.939

*SE - standard error; R^2 - coefficient of determination

Values of determined k and $t_{1/2}$show reciprocal dependence on the TPM concentration. Kinetic curves for different TPM concentrations are similarly shaped and follow the pseudo first rate order. From the experimental results can be seen that it takes longer time for the first part of the reaction to take place (reduction of TPM concentration by 50 %), which indicates the persistence of the fungicide.

3. 2. 3. Comparison of catalysts activities

The fabricated materials were utilized as photocatalysts with the aim to help in the degradation of the chosen pollutant. Figure 9 depicts a comparison of photocatalysts efficiencies toward the decomposition of TPM in water solution under simulated solar light.

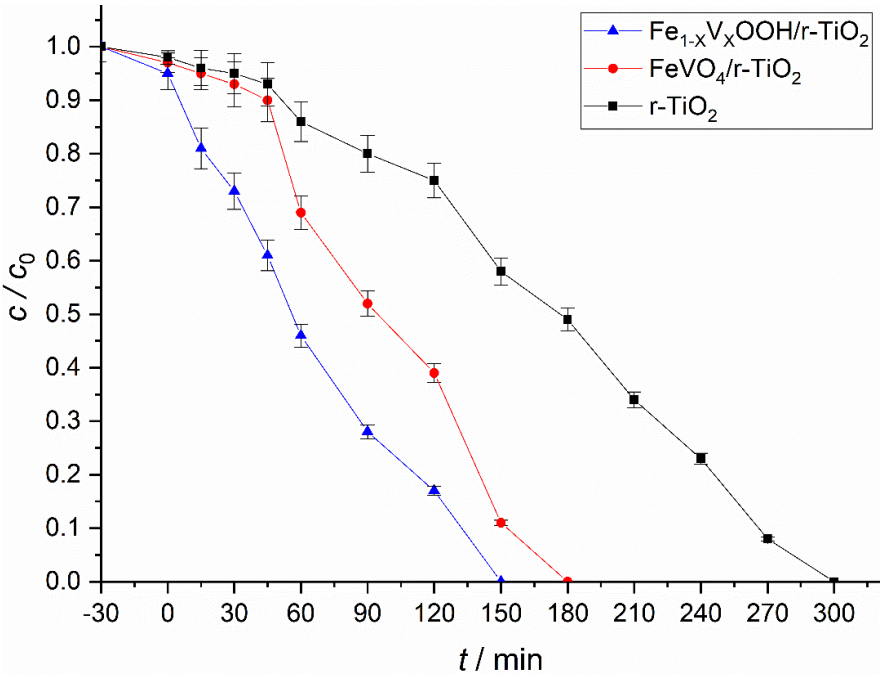

Figure 9. Photocatalytic activity of prepared materials and commercial r-TiO_2 (150 mL of suspension mixing at 200 rpm in the dark for the first 30 min, after that mixing under irradiation using 0.067 g L^{-1} of the selected photocatalyst)

As can be observed, the $Fe_{1-x}V_xOOH$-modified catalyst has shown the best performance. The base material r-TiO_2 shows the weakest ability to advance photodegradation, which justifies the fact that further modification of the surface

was necessary. Worse outcomes can be explained by the fact that TiO_2 absorbs only in the UV area of radiation [37,38]. Contrarily, molecules of vanadium oxide and vanadium oxyhydroxide can be excited by solar radiation. This is the reason for better activity and lower degradation times in cases when this two photocatalysts were employed ($FeVO_4$/r-TiO_2 and $Fe_{1-x}V_xOOH$/r-TiO_2). Increased generation of photoactive species significantly impacted photocatalytic degradation, and this could be another explanation for better catalytic performances of the fabricated materials. Furthermore, it is necessary to put special effort into engineering of materials with the tunable gap energy, so that they can easily surpass all barriers for better charge transfer [39]. Once again it was proven that the band gap energy plays a special role in the field of radiation-assisted photocatalytic reactions.

3. 2. 4. Reusability

Efficiencies of materials in 5 consecutive exploited cycles are shown in Figure 10.

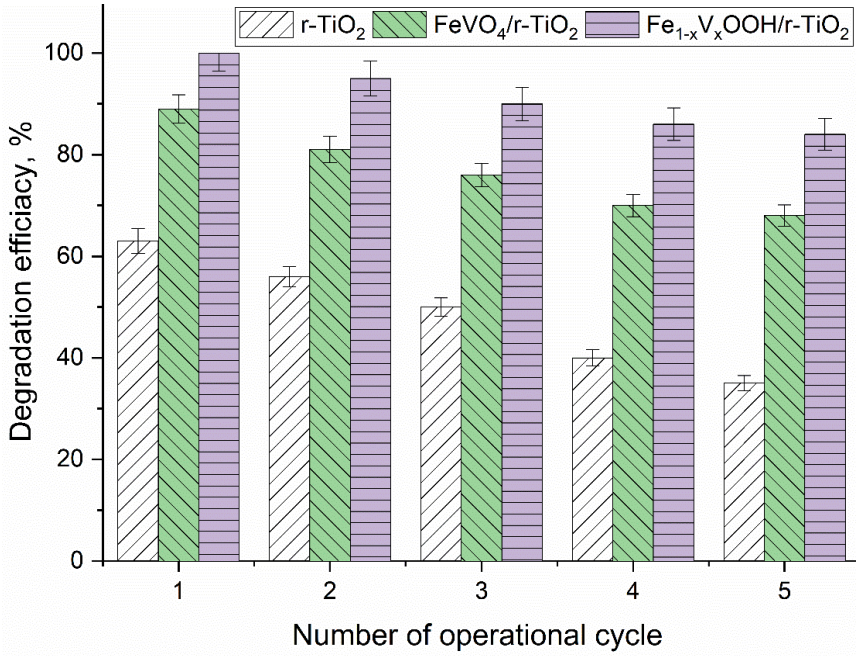

Figure 10. Multicycle efficiencies of catalysts ($c_{0(TPM)}$ = 5 mg L^{-1}, catalyst amount = 0.067 g L^{-1}, solution volume = 150 mL, 200 rpm, the cycle time for each degradation experiment was set to 150 min)

A slightly lower reusability potential of $FeVO_4$/r-TiO_2 with respect to $Fe_{1-x}V_xOOH$/r-TiO_2 was obtained, while the lowest was obtained for r-TiO_2. The gradual decrease of degradation power of all materials could be explained by the fact that some active sites lose their ability to generate oxidative species during the next cycles. Furthermore, possible reason can be infinitesimal peeling of the photocatalysts surface layer [40]. Also, another explanation can be the irreversible adsorption of whole or some TPM degradation products on the catalyst's surface. As a result, the photocatalyst surface became partly covered with some degradation products, which reduced the ability to degrade the target compound [41].The material with the least reduced catalytic activity was $Fe_{1-x}V_xOOH$/r-TiO_2.

3. 3. Chemical oxygen demand

Measuring of COD represents one of the key factors in determining whether wastewater can be discharged into a recipient. The obtained results of COD under the optimized conditions are represented in Table 2 together with standard deviation (SD) values.

The values of COD are constantly decreasing during the degradation time which is in accordance with degradation kinetics (see 3.2.3. subchapter). Considering that the maximum permissible concentration of this pesticide in water is not regulated, monitoring of COD is of crucial importance. The initial value was lowered more than 10 times for the proposed irradiation period, and once again demonstrated the effectiveness of the fabricated composite.

Table 2. Measured COD values for TPM solution obtained in the course of the photocatalytic degradation (c_0 = 5 mg L^{-1}, 0.067 g L^{-1} of $Fe_{1-x}V_xOOH/r\text{-}TiO_2$, COD data is the triplicate measurement average)

Time, min	0	30	60	90	120	150	180
COD , mg L^{-1}	1255	1100	1000	830	480	260	100
SD (COD), mg L^{-1}	7.348	8.165	4.082	5.715	7.348	4.899	1.633

As mentioned before, the overall process has to be considered from the aspect of material costs on the global market. Sustainability and possibility for practical application highly depend on all process costs. Prices for chosen micro- and nanosized compounds for the synthesis of photocatalysts are shown in Table 3.

Table 3. Comparison of prices for commercially available compounds for synthesis of photocatalysts [42]

Compound	Price of microsize, € per 100 g	Price of nanosize, € per 100 g
r, a-TiO_2	-	316.00
r-TiO_2	145.00	261.00
a-TiO_2	32.30	476.00
ZnO	15.50	253.20
CdS	105.20	-
MoS_2	73.00	2230.00
WO_3	1180.00	2610.00

It is clear that materials in the form of nanosized particles are more expensive than the microsized ones. That is the main reason for possible use of microsize photocatalyst based on r-TiO_2. Also, high abundance and availability of this material in nature together with good performances make rutile-phased TiO_2 a simple choice. Modified TiO_2-based composites are not much more expensive. Costs of auxiliary chemicals are: $Fe(NO_3)_3{\times}9H_2O$ (49.00 € for 100 g), VCl_3 (502 € for 100 g), NH_4VO_3(48.00 € for 100 g), KOH (6.10 € for 100 g). Bearing in mind that the deposited amount of$FeVO_4$or $Fe_{1-x}V_xOOH$ is up to 10 wt.% and considering the molar ratio of mentioned reagents during the preparation of the catalyst, the justification of the synthesis of new catalysts can be confirmed.

4. CONCLUSION

Global pollution is a widespread problem with broad spectrum of negative influences on society. Wastewater treatment in conventional processes often cannot solve the issue of pollutant removal on proper and sustainable way. Therefore, oxidative processes such as photocatalysis are attracting more and more attention for applications in real systems. From results obtained by detailed investigations in this study, the following outcomes can be drawn.

1. Structural methods for materials characterization prove successful and uniform deposition of $FeVO_4$ and $Fe_{1-x}V_xOOH$ onto r-TiO_2 surface up to 5.5 wt.%.
2. Nanosized particles significantly improved the oxidative abilities of the composite by reducing band gap energies (2.68 and 2.87 eV for $Fe_{1-x}V_xOOH/r\text{-}TiO_2$ and $FeVO_4/r\text{-}TiO_2$, respectively).
3. The prepared photocatalysts have shown better photocatalytic performances toward TPM degradation subjected to artificial sunlight irradiation (reduced degradation half time) than non-modified r-TiO_2, and all processes follow the pseudo-first rate order kinetics.
4. Determined optimal conditions for degradation reaction are 0.07 g L^{-1} of catalyst and 5 mg L^{-1} of TPM water solution.
5. A slight decrease in the photocatalytic activity was observed during a 5-cycle exploitation, with the most stable being $Fe_{1-x}V_xOOH/r\text{-}TiO_2$.
6. COD values implied that the proposed treatment was effective (more than 10 times decreased value, under the legislation value).

Based on the described conclusions, it was shown that the fabricated composite photocatalysts are valuable to be applied for TPM photodegradation. Future considerations should be focused on the scale up of the laboratory process to the pilot level with feasibility studies.

Acknowledgements: This work was supported by the Ministry of Science, Technological Development and Innovation of the Republic of Serbia (Contract Nos. 451-03-47/2023-01/200023; 451-03-9/2023-14/200017; 451-03-47/2023-01/200135).

REFERENCES

[1] Schaider LA, Rodgers KM, Rudel RA. Review of Organic Wastewater Compound Concentrations and Removal in Onsite Wastewater Treatment Systems. *Environ Sci Technol.* 2017; 51(13): 7304-7317. https://doi.org/10.1021/acs.est.6b04778

[2] Syafrudin M, Kristanti RA, Yuniarto A, Hadibarata T, Rhee J, Al-Onazi WA, Algarni TS, Almarri AH, Al-Mohaimeed AM. Pesticides in drinking water-a review. *Int J Environ Res Public Health.* 2021; 18(2): 468. https://doi.org/10.3390/ijerph18020468

[3] Hassaan MA, El Nemr A. Pesticides pollution: Classifications, human health impact, extraction and treatment techniques. *Egypt J Aquat Res.* 2020; 46(3): 207-220. https://doi.org/10.1016/j.ejar.2020.08.007

[4] Jatoi AS, Hashmi Z, Adriyani R, Yuniarto A, Mazari SA, Akhter F, Mubarak NM. Recent trends and future challenges of pesticide removal techniques – A comprehensive review. *J Environ Chem Eng.* 2021; 9(4): 105571. https://doi.org/10.1016/j.jece.2021.105571

[5] Leong WH, Teh SY, Hossain MM, Nadarajaw T, Zabidi-Hussin Z, Chin SY, Lai KS, Lim SHE. Application, monitoring and adverse effects in pesticide use: The importance of reinforcement of Good Agricultural Practices (GAPs). *J Environ Manage.* 2020; 260 109987. https://doi.org/10.1016/j.jenvman.2019.109987

[6] Venugopal D, Karunamoorthy P, Beerappa R, Sharma D, Aambikapathy M, Rajasekar K, Gaikwad A, Kondhalkar S. Evaluation of work place pesticide concentration and health complaints among women workers in tea plantation, Southern India. *J Expo Sci Environ Epidemiol.* 2021; 31(3): 560-570. https://doi.org/10.1038/s41370-020-00284-3

[7] Che X, Huang Y, Zhong K, Jia K, Wei Y, Meng Y, Yuan W, Lu H. Thiophanate-methyl induces notochord toxicity by activating the PI3K-mTOR pathway in zebrafish (Danio rerio) embryos. *Environ Pollut.* 2023; 318: 120861. https://doi.org/10.1016/j.envpol.2022.120861

[8] Arena M, Auteri D, Barmaz S, Bellisai G, Brancato A, Brocca D, Bura L, Byers H, Chiusolo A, Court Marques D, Crivellente F, De Lentdecker C, Egsmose M, Erdos Z, Fait G, Ferreira L, Goumenou M, Greco L, Ippolito A, Istace F, Jarrah S, Kardassi D, Leuschner R, Lythgo C, Magrans JO, Medina P, Miron I, Molnar T, Nougadere A, Padovani L, Parra Morte JM, Pedersen R, Reich H, Sacchi A, Santos M, Serafimova R, Sharp R, Stanek A, Streissl F, Sturma J, Szentes C, Tarazona J, Terron A, Theobald A, Vagenende B, Verani A, Villamar-Bouza L. Peer review of the pesticide risk assessment of the active substance thiophanate-methyl. *EFSA J.* 2018; 16(5): e05133. https://doi.org/10.2903/j.efsa.2018.5133

[9] European Commission, Commission Implementing Regulation (EU) 2020/1498 concerning the non-renewal of approval of the active substance thiophanate-methyl, in accordance with Regulation (EC) No 1107/2009 of the European Parliament and of the Council concerning the placing of plant protection products on the market, and amending the Annex to Commission Implementing Regulation (EU) No 540/2011. *OJEU*. 2020; https://eur-lex.europa.eu/legal-content/EN/TXT/PDF/?uri=CELEX:32020R1498 (accessed December 12, 2022)

[10] Tan H, Li Q, Zhang H, Wu C, Zhao S, Deng X, Li Y. Pesticide residues in agricultural topsoil from the Hainan tropical riverside basin: Determination, distribution, and relationships with planting patterns and surface water. *Sci Tot Environ.* 2020; 722: 137856. https://doi.org/10.1016/j.scitotenv.2020.137856

[11] Saleh IA, Zouari N, Al-Ghouti MA. Removal of pesticides from water and wastewater: Chemical, physical and biological treatment approaches. *Environ Technol Innov.* 2020; 19: . https://doi.org/10.1016/j.eti.2020.101026

[12] Mukherjee A, Mehta R, Saha S, Bhattacharya A, Biswas PK, Kole RK. Removal of multiple pesticide residues from water by low-pressure thin-film composite membrane. *Appl Water Sci.* 2020; 10(12): 1-8. https://doi.org/10.1007/s13201-020-01315-y

[13] Jovanović AA, Bugarčić MD, Marinković AD, Sokić MD. Insights into the application of polyaniline-based composites in environmental engineering. *Metal Mater Data.* 2023; 1(1): 25-31. https://doi.org/10.30544/MMD1

[14] Zhang F, Wang X, Liu H, Liu C, Wan Y, Long Y, Cai Z. Recent advances and applications of semiconductor photocatalytic technology. *Appl Sci.* 2019; 9(12): 1-43. https://doi.org/10.3390/app9122489

[15] Shokri A, Sanavi Fard M. A critical review in the features and application of photocatalysts in wastewater treatment. *Chem Paper.* 2022; 76(9): 5309-5339. https://doi.org/10.1007/s11696-022-02256-3

[16] Zhang Y, Chu W. Cooperation of multi-walled carbon nanotubes and cobalt doped TiO2 to activate peroxymonosulfate for antipyrine photocatalytic degradation. *Sep Purif Technol.* 2022; 282: 119996. https://doi.org/10.1016/j.seppur.2021.119996

[17] He X, Kai T, Ding P. Heterojunction photocatalysts for degradation of the tetracycline antibiotic: a review. *Environ Chem Lett.* 2021; 19(6): 4563-4601. https://doi.org/10.1007/s10311-021-01295-8

[18] Low J, Yu J, Jaroniec M, Wageh S, Al-Ghamdi AA. Heterojunction Photocatalysts. *Adv Mat.* 2017; 29(20): 1601694. https://doi.org/10.1002/adma.201601694

[19] Xu J, Zhang T. Fabrication of spent FCC catalyst composites by loaded V2O5 and TiO2 and their comparative photocatalytic activities. *Sci Rep.* 2019; 9(1):11099. https://doi.org/10.1038/s41598-019-47155-y

[20] Kesavan G, Pichumani M, Chen SM. Influence of Crystalline, Structural, and Electrochemical Properties of Iron Vanadate Nanostructures on Flutamide Detection. *ACS Appl Nano Mater.* 2021; 4(6): 5883-5894. https://doi.org/10.1021/acsanm.1c00802
[21] Dutta DP, Ramakrishnan M, Roy M, Kumar A. Effect of transition metal doping on the photocatalytic properties of FeVO4 nanoparticles. *J Photochem Photobiol A Chem.* 2017; 335: 102-111. https://doi.org/10.1016/j.jphotochem.2016.11.022
[22] Min YL, Zhang K, Chen YC, Zhang YG. Synthesis of novel visible light responding vanadate/TiO2 heterostructure photocatalysts for application of organic pollutants. *Chem Eng J.* 2011; 175(1): 76-83. https://doi.org/10.1016/j.cej.2011.09.042
[23] Schwertman U, Cornell RM. Iron Oxides in the Laboratory. Second edition. Weinheim: Wiley VCH Verlag GmbH; 2000, 91-92.
[24] Ines M, Paolo P, Roberto F, Mohamed S. Experimental studies on the effect of using phase change material in a salinity-gradient solar pond under a solar simulator. *Sol Energy.* 2019; 186: 335-346. https://doi.org/10.1016/j.solener.2019.05.011
[25] EPA. Method 410.4, Revision 2.0: The Determination of Chemical Oxygen Demand by Semi-Automated Colorimetry. 1993
[26] Ozer D, Tunca ET, Oztas NA. Effects of fuel type on iron vanadate nanocatalyst synthesized by solution combustion method for methylene blue degradation. *J Nanopartcl Res.* 2021; 23(8): 1- 12. https://doi.org/10.1007/s11051-021-05303-4
[27] Zhao Y, Yao K, Cai Q, Shi Z, Sheng M, Lin H, Shao M. Hydrothermal route to metastable phase FeVO4 ultrathin nanosheets with exposed {010} facets: Synthesis, photocatalysis and gas-sensing. *Cryst Eng Comm*- 2014; 16(2): 270-276. https://doi.org/10.1039/c3ce41692e
[28] Cui Y, Xue Y, Zhang R, Zhang J, Li X, Zhu X. Vanadium-cobalt oxyhydroxide shows ultralow overpotential for the oxygen evolution reaction. *J Mater Chem A Mater.* 2019; 7(38):21911-21917. https://doi.org/10.1039/c9ta07918a
[29] Tamirat AG, Su WN, Dubale AA, Chen HM, Hwang BJ. Photoelectrochemical water splitting at low applied potential using a NiOOH coated codoped (Sn, Zr) α-Fe2O3 photoanode. *J Mater Chem A Mater.* 2015; 3(11): 5949-5961. https://doi.org/10.1039/c4ta06915c
[30] Frison R, Cernuto G, Cervellino A, Zaharko O, Colonna GM, Guagliardi A, Masciocchi N. Magnetite-maghemite nanoparticles in the 5-15 nm range: Correlating the core-shell composition and the surface structure to the magnetic properties. A total scattering study. *Chem Mat.* 2013; 25(23): 4820-4827. https://doi.org/10.1021/cm403360f
[31] Nithya VD, Selvan RK, Sanjeeviraja C, Radheep DM, Arumugam S. Synthesis and characterization of FeVO4 nanoparticles. *Mater Res Bull.* 2011; 46(10): 1654-1658. https://doi.org/10.1016/j.materresbull.2011.06.005
[32] Zhu X, Chen J, Yu X, Zhu X, Gao X, Cen K. Controllable synthesis of novel hierarchical V2O5/TiO2 nanofibers with improved acetone oxidation performance. *RSC Adv.* 2015; 5(39): 30416-30424. https://doi.org/10.1039/c5ra01001b
[33] Ghiyasiyan-Arani M, Salavati-Niasari M, Masjedi-Arani M, Mazloom F. An easy sonochemical route for synthesis, characterization and photocatalytic performance of nanosized FeVO4 in the presence of aminoacids as green capping agents. *J Mater Sci: Mater Electron.* 2018; 29(1): 474-485. https://doi.org/10.1007/s10854-017-7936-9
[34] George S, Pokhrel S, Ji Z, Henderson BL, Xia T, Li L, Zink JI, Nel AE, Mädler L. Role of Fe doping in tuning the band gap of TiO2 for the photo-oxidation-induced cytotoxicity paradigm. *J Am Chem Soc.* 2011; 133(29): 11270-11278. https://doi.org/10.1021/ja202836s
[35] Jovanović A, Stevanović M, Barudžija T, Cvijetić I, Lazarević S, Tomašević A, Marinković A. Advanced technology for photocatalytic degradation of thiophanate-methyl: Degradation pathways, DFT calculations and embryotoxic potential. *Process Saf Environ Prot.* 2023; 178: 423-443. https://doi.org/10.1016/j.psep.2023.08.054
[36] Lewis KA, Tzilivakis J, Warner DJ, Green A. An international database for pesticide risk assessments and management. *Hum Ecol Risk Assess.* 2016; 22(4): 1050-1064. https://doi.org/10.1080/10807039.2015.1133242
[37] Yoon H, Kim D, Park M, Kim J, Kim J, Srituravanich W, Shin B, Jung Y, Jeon S. Extraordinary Enhancement of UV Absorption in TiO2 Nanoparticles Enabled by Low-Oxidized Graphene Nanodots. *J Phys Chem C.* 2018; 122(22): 12114-12121. https://doi.org/10.1021/acs.jpcc.8b03329
[38] Alamelu K, Jaffar Ali BM. TiO2-Pt composite photocatalyst for photodegradation and chemical reduction of recalcitrant organic pollutants. *J Environ Chem Eng.* 2018; 6(5): 5720-5731. https://doi.org/10.1016/j.jece.2018.08.042
[39] Gonçalves JM, Ireno Da Silva M, Angnes L, Araki K. Vanadium-containing electro and photocatalysts for the oxygen evolution reaction: A review. *J Mater Chem A Mater.* 2020; 8(5): 2171-2206. https://doi.org/10.1039/c9ta10857b
[40] Sindhu AS, Shinde NB, Harish S, Navaneethan M, Eswaran SK. Recoverable and reusable visible-light photocatalytic performance of CVD grown atomically thin MoS2 films. *Chemosphere.* 2022; 287: 132347. https://doi.org/10.1016/j.chemosphere.2021.132347
[41] Guo T, Yang S, Chen Y, Yang L, Sun Y, Shang Q. Photocatalytic kinetics and cyclic stability of photocatalysts Fe-complex/TiO2 in the synergistic degradation of phenolic pollutants and reduction of Cr(VI). *Environ Sci Pollut Res.* 2021; 28(10): 12459-12473. https://doi.org/10.1007/s11356-020-11220-1
[42] Sigma Aldrich 2023. https://www.sigmaaldrich.com/RS/en/search (accessed May 22, 2023)

Fotodegradacija tiofanat-metila pod dejstvom svetlosti koja imitira sunčevo zračenje korišćenjem novih kompozitnih fotokatalizatora

Aleksandar A. Jovanović[1], Mladen D. Bugarčić[1], Miroslav D. Sokić[1], Tanja S. Barudžija[2], Vladimir P. Pavićević[3] i Aleksandar D. Marinković[3]

[1]Institut za tehnologiju nuklearnih i drugih mineralnih sirovina, Beograd, Srbija
[2]Univerzitet u Beogradu, Institut za nuklearne nauke "Vinča" - Institut od nacionalnog značaja, Beograd, Srbija
[3]Univerzitet u Beogradu, Tehnološko-metalurški fakultet, Beograd, Srbija

(Naučni rad)

Izvod

Ovaj rad ima za cilj da prikaže uticaj prisustva nanočestica na površini titanijum (IV) oksida na fotokatalitički kapacitet razlaganja prisutnog organskog polutanta pod dejstvom simulirane sunčeve svetlosti. U tu svrhu, površina rutil titanijum (IV) oksida (r-TiO_2) dekorisana je železo vanadatom ($FeVO_4$/r-TiO_2) i vanadijumom supstituisanim getitom ($Fe_{1-x}V_xOOH$/r-TiO_2). Dobijeni kompoziti su okarakterisani primenom skenirajuće elektronske mikroskopije u emisionom polju uz energetsku disperzionu spektroskopiju, difrakcije X-zraka na sprašenim uzorcima, adsorpcijom azota na tački ključanja primenom Brunauer-Emet-Teler metodologije, infracrvene spektroskopije sa Furijeovom transformacijom u modu smanjene totalne refleksije i spektroskopije difuzne refleksije ultraljubičasto-vidljivog zračenja. Oba fotokatalizatora su pokazala veću fotoaktivnost od komercijalnog r-TiO_2 za degradaciju tiofanat-metila (2,5 h umesto 5 h). Tokom ispitivanja ispitivani su faktori kao što su vreme zračenja, količina katalizatora i koncentracija pesticida. Takođe, fotokatalizatori su primenjeni u uzastopnim višecikličnim testovima degradacije da bi se ispitala njihova efikasnost tokom dužeg vremena eksploatacije. Praćenje brzine uklanjanja vršeno je pomoću spektrometrije ultraljubičastog/vidljivog zračenja i tečne hromatografije visokih performansi. Pomoćni alat za proveru potpunosti razgradnje fungicida jeste određivanje hemijske potrošnje kiseonika nakon svake faze tretmana. Koncentracija posmatrane zagađujuće materije u tretiranim uzorcima je ispod propisanog zakonskog nivoa. Pripremljeni materijali su pokazali veliku stabilnost, postojanost i fotokatalitičku aktivnost što predstavlja dobru osnovu za primenu ovog procesa u realnim postrojenjima za prečišćavanje otpadnih voda.

Ključne reči: fotokataliza; titanijum (IV) oksid; unapređeni oksidacioni procesi; zagađenje pesticidima; otpadne vode